DESY 00-098
UWThPh-2000-25
WUE-ITP-2000-016
HEPHY-PUB 731/2000
hep-ph/xxxxxxx

Impact of e^+ and e^- Beam Polarization on Chargino and Neutralino Production at a Linear Collider

G. Moortgat–Pick[a1], A. Bartl[b2], H. Fraas[c3], W. Majerotto[d4]

[a] *DESY, Deutsches Elektronen–Synchrotron, D–22603 Germany*
[b] *Institut für Theoretische Physik, Universität Wien, A–1090 Wien, Austria*
[c] *Institut für Theoretische Physik, Universität Würzburg, D–97074 Würzburg, Germany*
[d] *Institut für Hochenergiephysik der Österreichischen Akademie der Wissenschaften, A–1050 Wien, Austria*

Abstract

We study the production processes $e^+e^- \to \tilde{\chi}_i^+\tilde{\chi}_j^-$, $i,j = 1,2$, and $e^+e^- \to \tilde{\chi}_m^0\tilde{\chi}_n^0$, $m,n = 1,\ldots,4$, working out the advantages of polarizing both beams. For $e^+e^- \to \tilde{\chi}_1^+\tilde{\chi}_1^-$ with $\tilde{\chi}_1^- \to \tilde{\chi}_1^0 e^-\bar{\nu}$ and $e^+e^- \to \tilde{\chi}_1^0\tilde{\chi}_2^0$ with $\tilde{\chi}_2^0 \to \tilde{\chi}_1^0 e^+e^-$ we perform a detailed analysis, including the complete spin correlations between production and decay. We analyze the forward–backward asymmetry of the decay electron for various beam polarizations. We also study polarization asymmetries in $e^+e^- \to \tilde{\chi}_1^0\tilde{\chi}_2^0$. These asymmetries strongly constrain the gaugino parameter M_1 and the masses $m_{\tilde{e}_L}$, $m_{\tilde{e}_R}$, $m_{\tilde{\nu}}$ also if $m_{\tilde{e},\tilde{\nu}} \geq \sqrt{s}/2$. We give numerical predictions for three scenarios for a linear collider with $\sqrt{s} = 500 - 1000$ GeV.

[1]e-mail: gudrid@mail.desy.de
[2]e-mail: bartl@ap.univie.ac.at
[3]e-mail: fraas@physik.uni-wuerzburg.de
[4]e-mail: majer@hephy.oeaw.ac.at.

1 Introduction

The search for supersymmetric (SUSY) particles and the determination of their properties will be one of the main goals of a future e^+e^- linear collider. Particularly interesting will be the experimental study of charginos and neutralinos, which are the quantum mechanical mixtures of the charged and neutral gauginos and higgsinos, the SUSY partners of the charged and neutral gauge and Higgs bosons. In the Minimal Supersymmetric Standard Model (MSSM) there are two charginos $\tilde{\chi}_i^{\pm}$, $i = 1, 2$, and four neutralinos $\tilde{\chi}_i^0$, $i = 1, \ldots, 4$. Usually the lightest neutralino $\tilde{\chi}_1^0$ is the lightest SUSY particle LSP. The masses and couplings of the charginos are determined by the SUSY parameters M_2, μ and $\tan\beta$. The neutralino properties depend in addition on the gaugino mass parameter M_1. An e^+e^- linear collider, where charginos and neutralinos can be pair produced, will allow a precise determination of the SUSY parameters involved.

Previous papers mainly analyzed production cross sections and decay branching ratios in the MSSM (see, e.g. [1, 2] and references therein). Recently a method for determining the SUSY parameters M_2, μ and $\tan\beta$ by measuring suitable observables in chargino production $e^+e^- \to \tilde{\chi}_i^+\tilde{\chi}_j^-$ $(i, j = 1, 2)$ has been proposed [3]. The gaugino mass parameter M_1 can in principle be determined from the neutralino mass spectrum [3, 4]. Models with an extended neutralino sector have been discussed in [5, 6]. A detailed study of the neutralino system is also helpful for examining the question whether the MSSM or another SUSY model is realized in nature.

In the present paper we study the production and decay of charginos and neutralinos with both the e^- and the e^+ beam polarized. We show that suitably polarizing both beams has three advantages: One can gain higher cross sections and thereby reduce the experimental errors. By measuring suitable observables one can get additional information on the mixing components of charginos and neutralinos as well as on the masses of the exchanged $\tilde{\nu}_e$, $\tilde{e}_L$, $\tilde{e}_R$. Moreover, the background can be reduced by appropriately polarizing the beams.

In the calculation of the decay angular distributions one has to take into account the spin correlations between production and decay of the charginos and neutralinos. They are particularly important near threshold. The processes $e^+e^- \to \tilde{\chi}_i^+\tilde{\chi}_j^-$, $\tilde{\chi}_i^+ \to \tilde{\chi}_k^0\ell^+\nu$ and $e^+e^- \to \tilde{\chi}_i^0\tilde{\chi}_j^0$, $\tilde{\chi}_i^0 \to \tilde{\chi}_k^0\ell^+\ell^-$, including the full spin correlations, have been studied in [7, 8]. In [9, 10] we have given the complete analytical formulae for longitudinally e^- and e^+ polarized beams in the laboratory system.

In our numerical analysis we will consider three scenarios, where $\tilde{\chi}_{1,2}^0$,

$\tilde{\chi}_1^\pm$ are gaugino–like and which differ in $\tan\beta$ and the selectron masses. We analyze the e^- and e^+ polarization dependence of all production sections accessible at a linear collider in the 500-1000 GeV range. In the case of $\tilde{\chi}_1^+\tilde{\chi}_1^-$ pair production and associated $\tilde{\chi}_1^0\tilde{\chi}_2^0$ production we study the dependence of the cross section and the forward–backward asymmetry of the decay electron on the beam polarizations and on the masses of the exchanged $\tilde{\nu}$, $\tilde{e}_L$ and $\tilde{e}_R$. We also relax the GUT relation between M_1 and M_2, $M_1/M_2 = \frac{5}{3}\tan^2\Theta_W$, and study the M_1 dependence of the forward-backward asymmetry of the decay electron and the polarization asymmetry.

2 Spin Correlations between Production and Decay

The helicity amplitudes for the production processes

$$e^+e^- \to \tilde{\chi}_i^+\tilde{\chi}_j^-, \tag{1}$$
$$e^+e^- \to \tilde{\chi}_i^0\tilde{\chi}_j^0, \tag{2}$$

are denoted by $T_P^{\lambda_i\lambda_j}$ and those for the decay processes

$$\tilde{\chi}_i^+ \to \tilde{\chi}_k^0\ell^{+\,(-)}_{\nu_\ell}, \tag{3}$$
$$\tilde{\chi}_i^0 \to \tilde{\chi}_k^0\ell^+\ell^- \tag{4}$$

by T_{D,λ_i} (and analogously T_{D,λ_j} for the decaying $\tilde{\chi}_j^-$ and $\tilde{\chi}_j^0$). The corresponding Feynman diagrams are given in Figs. 1a and b.

The amplitude squared of the combined process of production and decay is (summed over helicities):

$$|T|^2 = |\Delta(\tilde{\chi}_i)|^2|\Delta(\tilde{\chi}_j)|^2\rho_P^{\lambda_i\lambda_j\lambda_i'\lambda_j'}\rho_{D,\lambda_i'\lambda_i}\rho_{D,\lambda_j'\lambda_j}. \tag{5}$$

It is composed of the (unnormalized) spin density production matrix

$$\rho_P^{\lambda_i\lambda_j\lambda_i'\lambda_j'} = T_P^{\lambda_i\lambda_j}T_P^{\lambda_i'\lambda_j'*}, \tag{6}$$

the decay matrices

$$\rho_{D,\lambda_i'\lambda_i} = T_{D,\lambda_i}T^*_{D,\lambda_i'}, \quad \rho_{D,\lambda_j'\lambda_j} = T_{D,\lambda_j}T^*_{D,\lambda_j'}, \tag{7}$$

and the propagator

$$\Delta(\tilde{\chi}_k) = 1/[p_k^2 - m_k^2 + im_k\Gamma_k]. \tag{8}$$

Here p_k^2, λ_k, m_k and Γ_k denote the four–momentum squared, helicity, mass and total width of $\tilde{\chi}_k$. For this propagator we use the narrow–width approximation.

The density matrices can be expanded in terms of the Pauli matrices σ^a:

$$\begin{aligned}
\rho_P^{\lambda_i\lambda_j\lambda_i'\lambda_j'} &= (\delta_{\lambda_i\lambda_i'}\delta_{\lambda_j\lambda_j'}P(\tilde{\chi}_i\tilde{\chi}_j) + \delta_{\lambda_j\lambda_j'}\sum_{a=1}^{3}\sigma^a_{\lambda_i\lambda_i'}\Sigma_P^a(\tilde{\chi}_i) \\
&\quad +\delta_{\lambda_i\lambda_i'}\sum_{b=1}^{3}\sigma^b_{\lambda_j\lambda_j'}\Sigma_P^b(\tilde{\chi}_j) + \sum_{a,b=1}^{3}\sigma^a_{\lambda_i\lambda_i'}\sigma^b_{\lambda_j\lambda_j'}\Sigma_P^{ab}(\tilde{\chi}_i\tilde{\chi}_j)), \qquad (9)\\
\rho_{D,\lambda_i'\lambda_i} &= (\delta_{\lambda_i'\lambda_i}D(\tilde{\chi}_i) + \sum_{a=1}^{3}\sigma^a_{\lambda_i'\lambda_i}\Sigma_D^a(\tilde{\chi}_i)), \qquad (10)\\
\rho_{D,\lambda_j'\lambda_j} &= (\delta_{\lambda_j'\lambda_j}D(\tilde{\chi}_j) + \sum_{b=1}^{3}\sigma^b_{\lambda_j'\lambda_j}\Sigma_D^b(\tilde{\chi}_j)). \qquad (11)
\end{aligned}$$

We have chosen the polarization vectors such that $\Sigma_P^1(\tilde{\chi}_{i,j})$ describes the transverse polarization in the production plane, $\Sigma_P^2(\tilde{\chi}_{i,j})$ denotes the polarization perpendicular to the production plane and $\Sigma_P^3(\tilde{\chi}_{i,j})$ describes the longitudinal polarization of the chargino or neutralino, respectively. $\Sigma_P^{ab}(\tilde{\chi}_i\tilde{\chi}_j)$ is due to correlations between the polarizations of both charginos or neutralinos, respectively. The complete analytical expressions for the production density matrix and for the decay matrices are given in [7, 9].

The amplitude squared $|T|^2$ of the combined process of production and decay, eq. (5), can be rewritten as:

$$\begin{aligned}
|T|^2 = 4|\Delta(\tilde{\chi}_i)|^2|\Delta(\tilde{\chi}_j)|^2\Big(&P(\tilde{\chi}_i\tilde{\chi}_j)D(\tilde{\chi}_i)D(\tilde{\chi}_j) + \sum_{a=1}^{3}\Sigma_P^a(\tilde{\chi}_i)\Sigma_D^a(\tilde{\chi}_i)D(\tilde{\chi}_j) \\
&+ \sum_{b=1}^{3}\Sigma_P^b(\tilde{\chi}_j)\Sigma_D^b(\tilde{\chi}_j)D(\tilde{\chi}_i) + \sum_{a,b=1}^{3}\Sigma_P^{ab}(\tilde{\chi}_i\tilde{\chi}_j)\Sigma_D^a(\tilde{\chi}_i)\Sigma_D^b(\tilde{\chi}_j)\Big). \qquad (12)
\end{aligned}$$

The differential cross section is then given by

$$d\sigma_e = \frac{1}{2s}|T|^2(2\pi)^4\delta^4(p_1+p_2-\sum_i p_i)d\mathrm{lips}(p_3\ldots p_{10}), \qquad (13)$$

where $d\mathrm{lips}(p_3,\ldots,p_{10})$ is the Lorentz invariant phase space element.

If one neglects all spin correlations between production and decay only the first term in (12) contributes. The second and third term in (12) describe

the spin correlations between the production and the decay process. The last term is due to spin–spin correlations between both decaying charginos or neutralinos.

3 Numerical Analysis and Discussion

In the following analysis we use the MSSM [11] as our general framework. The masses and couplings of neutralinos and charginos are determined by the parameters M_1, M_2, μ, $\tan\beta$, which can be chosen real if CP violation is neglected. Moreover, one usually makes use of the GUT relation

$$M_1 = \frac{5}{3} M_2 \tan^2 \Theta_W. \tag{14}$$

The explicit expressions for the neutralino and chargino mass mixing matrices can be found in [1] (note that in Refs. [1, 7] the notation M' and M for M_1 and M_2 was used).

In our analysis we study chargino and neutralino production and decays in three scenarios, which we denote by A1, A2 and B. The corresponding parameters are given in Table 1. In scenario A1 one has $\tan\beta = 3$ and the masses $m_{\tilde{e}_L} = 176$ GeV, $m_{\tilde{e}_R} = 132$ GeV, $m_{\tilde{\nu}} = 161$ GeV [12]. In this scenario $\tilde{\chi}_1^0$ is $\tilde{B}$–like, $\tilde{\chi}_2^0$ is $\tilde{W}^3$–like, and $\tilde{\chi}_1^\pm$ is $\tilde{W}^\pm$–like and $\tilde{\chi}_2^\pm$ $\tilde{H}^\pm$–like. Scenario A2 differs from A1 only by the higher $\tilde{e}_L$ mass $m_{\tilde{e}_L} = 500$ GeV. In scenario B one has $\tan\beta = 30$ and $m_{\tilde{e}_L} = 217$ GeV, $m_{\tilde{e}_R} = 183$ GeV and $m_{\tilde{\nu}} = 202$ GeV [12]. In this scenario $\tilde{\chi}_1^0$, $\tilde{\chi}_2^0$ and $\tilde{\chi}_1^\pm$ are also gaugino–like.

3.1 Beam Polarization Effects in Chargino Production

We study the dependence of the cross sections $\sigma(e^+e^- \to \tilde{\chi}_i^+ \tilde{\chi}_j^-)$, $i,j = 1,2$, on the electron beam polarization P_{e^-} and positron beam polarization P_{e^+} (with $P_{e^\pm} = \{-1, 0, 1\}$ for {left–,un–, right–} polarized) at $\sqrt{s} = m_{\tilde{\chi}_i^+} + m_{\tilde{\chi}_j^-} + 10$ GeV for scenarios A1 and B. We choose $\sqrt{s}$ not too far from threshold, because the spin correlations to be discussed below are largest near threshold [7]. As an abbrevation we write in the following just the final state $\tilde{\chi}_i^+ \tilde{\chi}_j^-$ for the process $e^+e^- \to \tilde{\chi}_i^+ \tilde{\chi}_j^-$.

- $\tilde{\chi}_1^+ \tilde{\chi}_1^-$
  Scenario A1 (see Fig. 2a): Due to the $\tilde{\nu}_e$ exchange and the gaugino character of $\tilde{\chi}_1^\pm$ a left polarized electron beam and a right polarized positron beam lead to the largest cross section. For $P_{e^-} = -85\%$ and $P_{e^+} = +60\%$ we obtain 410 fb, which means that the cross section is

enhanced by a factor of about three with respect to unpolarized beams (Table 2).

Scenario B: One gets a similar dependence on the beam polarizations and the same enhancement factor as in scenario A1. With $P_{e^-} = -85\%$ and $P_{e^+} = +60\%$ a cross section of 709 fb is reached (Table 2).

- $\tilde{\chi}_1^\pm \tilde{\chi}_2^\mp$
  Scenario A1 (see Fig. 2b): In this case γ exchange does not contribute and $\tilde{\nu}_e$ exchange is suppressed due to the higgsino–like $\tilde{\chi}_2^-$. Therefore, right polarized electrons and left polarized positrons are favoured. Due to the different character of $\tilde{\chi}_1^+$ and $\tilde{\chi}_2^-$ the cross section is small and reaches only 6 fb with $P_{e^-} = +85\%$ and $P_{e^+} = -60\%$ (Table 2).

  Scenario B (see Fig. 2d): In this case somewhat higher cross sections of about 10 fb can be reached with $P_{e^-} = +85\%$ and $P_{e^+} = -60\%$.

- $\tilde{\chi}_2^+ \tilde{\chi}_2^-$
  Scenario A1 (see Fig. 2c): As $\tilde{\chi}_2^\pm$ is higgsino–like $\tilde{\nu}_e$ exchange is negligible. The cross section is enhanced if the electrons are left and the positrons are right polarized, mainly due to the $\gamma - Z^0$ interference. For $P_{e^-} = -85\%$ and $P_{e^+} = +60\%$ it is enhanced by a factor 2.5 and reaches 113 fb.

  Scenario B: One gets a similar dependence on the beam polarizations and the same enhancement factor as in scenario A1. With $P_{e^-} = -85\%$ and $P_{e^+} = +60\%$ a cross section of 194 fb is reached (Table 2).

A summary of our results for scenario A1 and B is given in Table 2.

Since $\tilde{\nu}_e$ exchange favours left polarized electron beams and right polarized positron beams, one expects for gaugino–like scenarios the following sequence of polarized cross sections [10, 13] (for $|P_{e^-}| = 85\%$ and $|P_{e^+}| = 60\%$):

$$\sigma^{-+} > \sigma^{-0} > \sigma^{00} > \sigma^{--} > \sigma^{++} > \sigma^{+0} > \sigma^{+-}. \tag{15}$$

Here $(-+)$ etc. denotes the sign of the electron polarization P_{e^-} and of the positron polarization P_{e^+}, respectively.

On the other hand, for pure higgsinos one would have due to Z^0 exchange

$$\sigma^{-+} > \sigma^{+-} > \sigma^{-0} > \sigma^{00} > \sigma^{+0} > \sigma^{--} > \sigma^{++}. \tag{16}$$

These orderings are also valid if the decays are included.

The relations (15), (16) are, however, modified by the γ exchange contribution. Nevertheless, one can get additional information by using polarized

electron *and* positron beams, because the sequences of polarized cross sections for gaugino–like and higgsino–like scenarios are different. If only the electron beam is polarized, one would obtain in both scenarios the same sequence of polarized cross sections, namely $\sigma^{-0} > \sigma^{00} > \sigma^{+0}$.

In scenarios A1 and B we get the results in Table 2 for $|P_{e^-}| = 85\%$ and $|P_{e^+}| = 60\%$ at $\sqrt{s} = m_{\tilde{\chi}_i^\pm} + m_{\tilde{\chi}_j^\pm} + 10$ GeV. For $e^+e^- \to \tilde{\chi}_1^+\tilde{\chi}_1^-$ the relation (15) is fulfilled. However, for $e^+e^- \to \tilde{\chi}_2^+\tilde{\chi}_2^-$ (higgsino–like $\tilde{\chi}_2^\pm$) the sequence is different from relation (16) due to γ exchange and in particular γZ^0 interference.

Usually, one defines an effective polarization

$$P_{eff} = \frac{P_{e^-} - P_{e^+}}{1 - P_{e^-}P_{e^+}} \quad . \tag{17}$$

The error of the effective polarization can be reduced when both beams are polarized.

3.2 Beam Polarization Effects in Neutralino Production

In this subsection we study the dependence of the cross section $\sigma(e^+e^- \to \tilde{\chi}_i^0\tilde{\chi}_j^0)$, $i,j = 1,\ldots,4$, on the longitudinal beam polarizations P_{e^-} and P_{e^+} at $\sqrt{s} = (m_{\tilde{\chi}_i^0} + m_{\tilde{\chi}_j^0}) + 30$ GeV, for scenario A1, A2 and B. In the following we again denote the production process $e^+e^- \to \tilde{\chi}_i^0\tilde{\chi}_j^0$ by its final state $\tilde{\chi}_i^0\tilde{\chi}_j^0$.

- $\tilde{\chi}_1^0\tilde{\chi}_2^0$
  Scenario A1 (see Fig. 3a): Since $\tilde{\chi}_1^0$ is mostly $\tilde{B}$–like and $\tilde{\chi}_2^0$ is mostly $\tilde{W}^3$–like mainly $\tilde{e}_L$ and $\tilde{e}_R$ exchange in the t– and u– channel contribute. One gets the largest cross section for left polarized electrons and right polarized positrons. Due to the strong $\tilde{B}$ component of $\tilde{\chi}_1^0$ one gets a slight enhancement also for right polarized electrons and left polarized positrons. For $P_{e^-} = -85\%$ and $P_{e^+} = +60\%$ the cross section goes up to 56 fb, which is larger by a factor of 1.8 than for unpolarized beams.

  Scenario A2 (see Fig. 3b): Since $m_{\tilde{e}_L} \gg m_{\tilde{e}_R}$ $\tilde{e}_L$ exchange is suppressed leading to an enhancement for right polarized electrons and left polarized positrons. With $P_{e^-} = +85\%$ and $P_{e^+} = -60\%$ one reaches 35 fb, that is an enhancement by a factor 2.7 with respect to unpolarized beams.

  Scenario B (see Fig. 3c): Due to the different couplings for large $\tan\beta$ the dependence on the beam polarizations slightly changes. For $P_{e^-} =$

-85% and $P_{e^+} = +60\%$ one has an enhancement factor of 2.4 with respect to the unpolarized case. The cross section reaches 50 fb.

- $\tilde{\chi}^0_2\tilde{\chi}^0_2$
  Scenario A1 (see Fig. 3d): Owing to the $\tilde{W}^3$ nature of $\tilde{\chi}^0_2$, the cross section is governed by $\tilde{e}_L$ exchange. Hence the cross section is largest for left polarized electrons and right polarized positrons. It reaches 121 fb for $P_{e^-} = -85\%$ and $P_{e^+} = +60\%$, which gives an enhancement by a factor of 3 with respect to unpolarized beams.

  Scenario B: One gets the same enhancement factor compared to the unpolarized case as in scenario A1. Due to the smaller lepton-slepton-neutralino couplings the cross sections are about a factor two smaller. For $P_{e^-} = -85\%$ and $P_{e^+} = +60\%$ one gets 59 fb.

- $\tilde{\chi}^0_1\tilde{\chi}^0_3$
  Scenario A1 (Fig. 4a): Since $\tilde{\chi}^0_1$ is $\tilde{B}$–like and $\tilde{\chi}^0_3$ is higgsino–like the cross sections are smaller than for $\tilde{\chi}^0_1\tilde{\chi}^0_2$ production, reaching only 25 fb. Due to the large $\tilde{\chi}^0_1 e\tilde{e}_R$ coupling one gets an enhancement by a factor of 2.7 for $P_{e^-} = +85\%$ and $P_{e^+} = -60\%$ compared with the unpolarized case.

  Scenario B: One gets a similar enhancement factor of about 2.8 as in scenario A1. Due to slightly larger $\tilde{\chi}^0_3 e\tilde{e}_R$ coupling the cross section is 42 fb for $P_{e^-} = +85\%$ and $P_{e^+} = -60\%$.

- $\tilde{\chi}^0_1\tilde{\chi}^0_4$
  One expects a behaviour similar to $e^+e^- \to \tilde{\chi}^0_1\tilde{\chi}^0_3$. In scenario A1 the cross sections are about a factor 3 smaller and in scenario B a factor 6, see Table 3.

- $\tilde{\chi}^0_2\tilde{\chi}^0_3$
  Scenario A1 (see Fig. 4b): Since the $\tilde{\chi}^0_2$ has a strong $\tilde{W}^3$ component one gets the largest cross sections with left polarized electrons and right polarized positrons. With $P_{e^-} = -85\%$ and $P_{e^+} = +60\%$ the cross section is enhanced by a factor of 2.6 and reaches 41 fb.

  Scenario B: Due to slightly larger $\tilde{\chi}^0_3$ couplings than in scenario A1 one gets a cross section of 79 fb for $P_{e^-} = -85\%$ and $P_{e^+} = +60\%$.

Table 3 gives a survey of all cross sections $e^+e^- \to \tilde{\chi}^0_i\tilde{\chi}^0_j$ (including the invisible channel $e^+e^- \to \tilde{\chi}^0_1\tilde{\chi}^0_1$) for different beam polarizations. Note the large cross sections for $e^+e^- \to \tilde{\chi}^0_3\tilde{\chi}^0_4$ due to the large Z^0 couplings to the higgsino components. In summary the cross sections can be enhanced

by a factor two to three by polarizing both beams. For pure gaugino–like neutralinos and $m_{\tilde{e}_L} \gg m_{\tilde{e}_R}$ ($m_{\tilde{e}_L} \ll m_{\tilde{e}_R}$), for $P_{e^-} = +1$, $P_{e^+} = -1$ ($P_{e^-} = -1$, $P_{e^+} = +1$) the cross section could even be enlarged by a factor 4. For pure higgsino–like neutralinos and $P_{e^-} = +1$, $P_{e^+} = -1$ ($P_{e^-} = -1$, $P_{e^+} = +1$) the enhancement factor is 1.7 (2.3) [10, 14].

If the polarizations of both beams are varied, the relative size of the cross sections strongly depends on the mixing character of both neutralinos and on the selectron masses [10]. In particular, for $e^+e^- \to \tilde{\chi}_i^0\tilde{\chi}_j^0$ and if $\tilde{\chi}_i^0$ and $\tilde{\chi}_j^0$ are pure higgsinos, one obtains for $|P_{e^-}| = 85\%$ and $|P_{e^+}| = 60\%$ the sequence

$$\sigma^{-+} > \sigma^{+-} > \sigma^{-0} > \sigma^{00} > \sigma^{+0} > \sigma^{--} > \sigma^{++}. \tag{18}$$

If $\tilde{\chi}_i^0$ and $\tilde{\chi}_j^0$ are pure gauginos, the order of the cross sections depends on the relative magnitude of the selectron masses $m_{\tilde{e}_L}$ and $m_{\tilde{e}_R}$. For $m_{\tilde{e}_L} \gg m_{\tilde{e}_R}$ only right selectron exchange contributes, and one obtains

$$\sigma^{+-} > \sigma^{+0} > \sigma^{00} > \sigma^{++} > \sigma^{--} > \sigma^{-0} > \sigma^{-+}, \tag{19}$$

whereas for $m_{\tilde{e}_R} \gg m_{\tilde{e}_L}$ (which may be realized in extended SUSY models, [6] and references therein), one gets:

$$\sigma^{-+} > \sigma^{-0} > \sigma^{00} > \sigma^{--} > \sigma^{++} > \sigma^{+0} > \sigma^{+-}. \tag{20}$$

A comparison of (18) and (20) shows that polarizing both beams allows one to distinguish between a higgsino–like scenario and a gaugino–like scenario with dominating $\tilde{e}_L$ exchange. This is not possible if only the electron beam is polarized.

From Table 3 one notices that for $e^+e^- \to \tilde{\chi}_3^0\tilde{\chi}_4^0$ one obtains the same ordering of the polarized cross sections in scenario A1 and B (with $\tilde{\chi}_3^0$ and $\tilde{\chi}_4^0$ higgsino–like) as in (18). Comparing the sequence of cross sections for $e^+e^- \to \tilde{\chi}_1^0\tilde{\chi}_2^0$ in scenario A2 (with $\tilde{\chi}_1^0$, $\tilde{\chi}_2^0$ gaugino–like) with (19), one observes the influence of $\tilde{e}_L$ exchange which is however suppressed due to the high mass $m_{\tilde{e}_L} = 500$ GeV.

3.3 Decay Lepton Forward–Backward Asymmetries

We will discuss the forward–backward asymmetry of the lepton angular distribution $d\sigma_e/d\cos\Theta_e$ in the overall c.m.s. of the combined reactions

$$e^+e^- \to \tilde{\chi}_1^+\tilde{\chi}_1^-, \qquad \tilde{\chi}_1^- \to \tilde{\chi}_1^0 e^-\bar{\nu} \tag{21}$$

and

$$e^+e^- \to \tilde{\chi}_1^0\tilde{\chi}_2^0, \qquad \tilde{\chi}_2^0 \to \tilde{\chi}_1^0 e^+e^-. \tag{22}$$

Here Θ_e denotes the angle between the electron beam and the decay electron e^-. The forward–backward asymmetry A_{FB} of the decay electron is defined as

$$A_{FB} = \frac{\sigma_e(\cos\Theta_e > 0) - \sigma_e(\cos\Theta_e < 0)}{\sigma_e(\cos\Theta_e > 0) + \sigma_e(\cos\Theta_e < 0)}, \tag{23}$$

where

$$\sigma_e = \sigma(e^+e^- \to \tilde{\chi}_1^+\tilde{\chi}_1^-) \times BR(\tilde{\chi}_1^- \to \tilde{\chi}_1^0 e^-\bar{\nu}) \tag{24}$$

for chargino production and decay and

$$\sigma_e = \sigma(e^+e^- \to \tilde{\chi}_1^0\tilde{\chi}_2^0) \times BR(\tilde{\chi}_2^0 \to \tilde{\chi}_1^0 e^+e^-) \tag{25}$$

for neutralino production and decay. Note that $d\sigma_e/d\cos\Theta_e$ and A_{FB} are sensitive to spin correlations.

The observable A_{FB}, eq. (23), is very sensitive to the gaugino component of the chargino/neutralino and the mass of the exchanged sneutrino or slepton. It has the advantage of being independent of the parameters of the squark sector which enter in σ_e, eqs. (24), (25), via the leptonic branching ratio, which cancels in eq. (23).

3.3.1 σ_e and A_{FB} in Chargino Production and Decay

Obviously, if the chargino $\tilde{\chi}_1^\pm$ has a substantial gaugino component, the sneutrino exchange in the t–channel has a strong influence on the cross section and angular distribution of chargino production. In [15, 16] the possibility of determining the sneutrino mass $m_{\tilde{\nu}_e}$ from the angular distribution of the production process $e^+e^- \to \tilde{\chi}_1^+\tilde{\chi}_1^-$ was studied. In the following we study the $m_{\tilde{\nu}_e}$ dependence of the decay lepton forward–backward asymmetry A_{FB}, eq. (23), in $e^+e^- \to \tilde{\chi}_1^+\tilde{\chi}_1^-$, $\tilde{\chi}_1^- \to \tilde{\chi}_1^0 e^-\bar{\nu}_e$ [7, 13]. As close to threshold this observable depends decisively on spin correlations, it is instructive to have a closer look on its $m_{\tilde{\nu}_e}$ dependence. A_{FB} also depends on the slepton mass $m_{\tilde{e}_L}$, due to the $\tilde{e}_L$ exchange in the decay amplitude. Since $\tilde{\ell}_L$ and $\tilde{\nu}_\ell$ are members of the same $SU(2)_L$ doublet, their masses are connected by the relation [16, 17]

$$m^2_{\tilde{\ell}_L} = m^2_{\tilde{\nu}_\ell} - m^2_W \cos 2\beta \tag{26}$$

with m_W the mass of the $W^\pm$ boson. Relation (26) is fulfilled at tree level, and is only modified by radiative corrections.

We first show in Fig. 5 the cross section σ_e, eq.(24), as a function of $m_{\tilde{\nu}_e}$ at $\sqrt{s} = 2m_{\tilde{\chi}_1^\pm} + 10$ GeV, fixing $m_{\tilde{e}_L}$ by eq. (26). σ_e exhibits a pronounced

minimum, which is due to the destructive interference between Z exchange and $\tilde{\nu}_e$ exchange [7]. For $\sqrt{s}$ near threshold this minimum is approximately at $m_{\tilde{\nu}_e} \approx m_{\tilde{\chi}_1^\pm}$ and in the limit $\sqrt{s} \to 2m_{\tilde{\chi}_1^\pm}$ the minimum reaches exactly $m_{\tilde{\nu}_e} \to m_{\tilde{\chi}_1^\pm}$. Due to this minimum there is an ambiguity when one tries to determine $m_{\tilde{\nu}_e}$ by measuring σ_e. At higher $\sqrt{s}$ the minimum is shifted to higher values of $m_{\tilde{\nu}}$ [10, 13].

In Fig. 6a and b we show the contour lines of A_{FB} as a function of $m_{\tilde{\nu}}$ and $m_{\tilde{e}_L}$ at $\sqrt{s} = 2m_{\tilde{\chi}_1^\pm} + 10$ GeV and $\sqrt{s} = 500$ GeV, respectively, for $P_{e^-} = -85\%$ and $P_{e^+} = +60\%$. In order to study separately the $m_{\tilde{\nu}_e}$ and $m_{\tilde{e}_L}$ dependence of A_{FB} we have relaxed the mass relation eq.(26). Apart from $m_{\tilde{\nu}}$ and $m_{\tilde{e}_L}$ the parameters are as in scenario A1. The large asymmetry is mainly due to $\tilde{\nu}_e$ exchange in the crossed channel of the production. Close to threshold also the $\tilde{e}_L$ exchange in the decay $\tilde{\chi}_1^- \to \tilde{\chi}_1^0 e^- \bar{\nu}_e$ plays an important role, see Fig. 6a. At energies far from threshold the charginos have a large energy, and the decay lepton has essentially the same direction as the chargino [18]. Therefore, the $\tilde{e}_L$ dependence is weaker [13], see Fig. 6b.

Due to the dominance of the t–channel contribution in scenario A1 the polarization dependence of the nominator and denominator in the ratio, eq. (23), almost cancels. Therefore A_{FB} depends only weakly on the polarizations of the beams.

Turning now to the question how accurate the sneutrino mass $m_{\tilde{\nu}_e}$ can be determined from chargino pair production and decay, Figs. 6a and b show that there is an appreciable $m_{\tilde{\nu}_e}$ dependence of A_{FB}. We first consider the case $m_{\tilde{\nu}_e} \gtrsim \sqrt{s}/2$, where $\tilde{\nu}_e \bar{\tilde{\nu}}_e$ pair production is kinematically not possible. We assume that the slepton mass $m_{\tilde{e}_L}$ and the other SUSY parameters are known with good precision. For definiteness, we take, $m_{\tilde{e}_L} = 200$ GeV, and the other SUSY parameters as in scenario A1.

At $\sqrt{s} = 500$ GeV, with a luminosity of $\mathcal{L} = 500$ fb^{-1}, A_{FB} can be measured up to $< \pm 1\%$, if we take only the statistical error $\delta(A_{FB})$. This means that in the range 350 GeV $\lesssim m_{\tilde{\nu}_e} \lesssim$ 800 GeV an accuracy of about $|\delta m_{\tilde{\nu}_e}| <$ 10 GeV may be achieved. The experimental errors of $m_{\tilde{e}_L}$ and the other SUSY parameters are neglected. The ambiguity at $\sqrt{s} = 500$ GeV (Fig. 6b) in the range 250 GeV $\lesssim m_{\tilde{\nu}_e} \lesssim$ 350 GeV can be resolved by measuring A_{FB} at different c.m.s. energies. Similarly, at $\sqrt{s} = 2m_{\tilde{\chi}_1^\pm} + 10$ GeV (Fig. 6a), A_{FB} is quite sensitive to $m_{\tilde{\nu}_e}$ in the range 135 GeV$\lesssim m_{\tilde{\nu}_e} \lesssim$350 GeV, where direct production is again not possible. If only the electron beam is polarized, $\delta(A_{FB})$ would be larger by about 20% in the case considered. Moreover, for $P_{e^-} = -85\%$ and $P_{e^+} = +60\%$ we obtain $P_{eff} = 96\%$. If P_{e^-} and P_{e^+} have an error of $\pm 1\%$, the error of P_{eff} would only be $\pm 0.83\%$. For a more

quantitative assessment of the accuracy of $m_{\tilde{\nu}_e}$ that can be expected from measuring the decay lepton forward–backward asymmetry in chargino production, Monte Carlo studies taking into account experimental cuts and detector simulation would be necessary. For instance a cut $-0.9 < \cos\Theta_e < 0.9$ would lead to about 10% smaller values of σ_e and A_{FB}.

In case $m_{\tilde{\nu}_e} < \sqrt{s}/2$, $\tilde{\nu}_e\bar{\tilde{\nu}}_e$ pairs can be directly produced. If $m_{\tilde{\chi}_1^\pm} < m_{\tilde{\nu}_e} < \sqrt{s}/2$, then the visible decay $\tilde{\nu}_e \to e^-\tilde{\chi}_1^+$ is kinematically allowed, and will presumably have a sufficiently high branching ratio. We do not treat this case here, because measuring the cross section of $e^+e^- \to \tilde{\nu}_e\bar{\tilde{\nu}}_e$ at threshold will allow us to determine $m_{\tilde{\nu}_e}$ with good accuracy [19]. If $m_{\tilde{\nu}_e} < m_{\tilde{\chi}_1^\pm} < \sqrt{s}/2$, then $\tilde{\nu}_e$ has no visible decay with sufficiently high branching ratio. However, the two–body chargino decay $\tilde{\chi}_1^\pm \to e^\pm \overset{(-)}{\tilde{\nu}}_e$ is possible. Measuring the endpoints of the energy spectrum of the decay leptons e^+ and e^- will provide a very precise determination of the masses $m_{\tilde{\chi}_1^\pm}$ and $m_{\tilde{\nu}_e}$. The alternative method to determine $m_{\tilde{\nu}_e}$ by measuring the decay lepton forward–backward asymmetry A_{FB} of chargino production will, in principle, also be possible. However, the accuracy of $m_{\tilde{\nu}_e}$ obtainable in this way is expected to be lower than that from the decay lepton energy spectrum.

3.3.2 A_{FB} in Neutralino Production and Decay

Owing to the Majorana character of the neutralinos the angular distribution of the production process is symmetric under the exchange $\cos\Theta \leftrightarrow -\cos\Theta$, where Θ is the production angle of $\tilde{\chi}_j^0$ [20]. The angular distribution of the decay lepton ℓ^-, however, depends on the polarization of $\tilde{\chi}_j^0$. Since the longitudinal polarization Σ_P^3 and the transverse polarization Σ_P^1 of $\tilde{\chi}_j^0$ are forward–backward antisymmetric, the lepton forward–backward asymmetry A_{FB} of the decay lepton, eq. (23), may become quite large. We will plot A_{FB} not too far from threshold because it decreases with $\sqrt{s}$ for fixed neutralino masses.

In Figs. 7a we show A_{FB} of the decay electron for reaction (22) as a function of the beam polarizations for scenario A1 at $\sqrt{s} = (m_{\tilde{\chi}_1^0} + m_{\tilde{\chi}_2^0}) +$ 30 GeV. As one can see, by appropriately polarizing both beams one gets a larger asymmetry. Note that in this scenario A_{FB} is practically zero if both beams are unpolarized.

In Figs. 7b and c we show the contour lines of A_{FB} as a function of $m_{\tilde{e}_L}$ and $m_{\tilde{e}_R}$ at $\sqrt{s} = m_{\tilde{\chi}_1^0} + m_{\tilde{\chi}_2^0} + 30$ GeV, for $P_{e^-} = -85\%$, $P_{e^+} = +60\%$ and $P_{e^-} = +85\%$, $P_{e^+} = -60\%$, respectively. The other parameters are as

in scenario A1. For $m_{\tilde{e}_L} \approx m_{\tilde{e}_R}$ the asymmetry A_{FB} is very small for both polarizations considered, but can reach approximately $\pm 23\%$ if $m_{\tilde{e}_L} \neq m_{\tilde{e}_R}$. Measuring the lepton forward–backward asymmetry A_{FB} in addition to the total cross section will give constraints on the selectron masses $m_{\tilde{e}_L}$ and $m_{\tilde{e}_R}$.

In the following we will estimate the precision to be expected if one tries to constrain the selectron masses by the data of A_{FB} of reaction (22). We assume that the right selectron mass is known with good precision and, for definiteness, we take $m_{\tilde{e}_R} = 240$ GeV. We further assume that the measurement of A_{FB} has given $A_{FB} = -10\%$ at $\sqrt{s} = m_{\tilde{\chi}^0_1} + m_{\tilde{\chi}^0_2} + 30$ GeV. For an integrated luminosity $\mathcal{L} = 500$ fb^{-1} the statistical error is expected to be $\delta(A_{FB}) \approx \pm 3\%$. Fig. 7b shows that, for $P_{e^-} = -85\%$ and $P_{e^+} = +60\%$, $m_{\tilde{e}_L}$ has to be either in the range 280 GeV$< m_{\tilde{e}_L} <$ 320 GeV or in 410 GeV$< m_{\tilde{e}_L} <$ 460 GeV. This example demonstrates that the mass of $\tilde{e}_L$ can be constrained by measuring A_{FB} even if it is too heavy to be directly produced in e^+e^- annihilation. As a second example we assume that $m_{\tilde{e}_R}$ is known to be $m_{\tilde{e}_R} = 340$ GeV, and $A_{FB} = +15\%$ has been measured. This constrains $m_{\tilde{e}_L}$ to be either in the mass region 250 GeV$< m_{\tilde{e}_L} <$ 300 GeV or in 450 GeV$< m_{\tilde{e}_L} <$ 600 GeV.

As in the chargino case, if both beams are polarized the cross sections can be enhanced and therefore the statistical error of A_{FB} can be reduced. Moreover, also the error of the effective polarization $\delta(P_{eff})$ can be reduced.

In [14] we also studied the $\sqrt{s}$ dependence of the lepton forward–backward asymmetry A_{FB}. For $\sqrt{s} \gg (m_{\tilde{\chi}^0_1} + m_{\tilde{\chi}^0_2})$ the angular distribution of the decay lepton is essentially the same as that of the neutralino $\tilde{\chi}^0_2$ [18]. Due to the Majorana character of the decaying neutralino $\tilde{\chi}^0_2$ the lepton forward–backward asymmetry now practically vanishes.

3.3.3 M_1 Dependence of σ_e, A_{FB} and A_{pol} in Neutralino Production and Decay

As is well known, the neutralino masses as well as the $Z^0\tilde{\chi}^0_i\tilde{\chi}^0_j$ couplings and the $\tilde{\chi}^0_i\tilde{\ell}\ell$ couplings also depend on the gaugino mass parameter M_1 [9, 14]. So far we have used the GUT relation (14) for the gaugino masses. In the following we will be more general and not use this relation [3, 4, 18, 21, 22]. We will discuss the M_1 dependence of the cross section, the polarization asymmetry and the forward–backward asymmetry of the decay electron [9, 14] in the reaction $e^+e^- \to \tilde{\chi}^0_1\tilde{\chi}^0_2$, $\tilde{\chi}^0_2 \to \tilde{\chi}^0_1 e^+e^-$. All other parameters are chosen as in scenario A1 except the mass of $\tilde{e}_R$, which we

take $m_{\tilde{e}_R} = 161$ GeV.

Fig. 8a exhibits the M_1 dependence of $\sigma(e^+e^- \to \tilde{\chi}_1^0\tilde{\chi}_2^0) \times BR(\tilde{\chi}_2^0 \to e^+e^-\tilde{\chi}_1^0)$ at $\sqrt{s} = (m_{\tilde{\chi}_1^0} + m_{\tilde{\chi}_2^0}) + 30$ GeV for $m_{\tilde{e}_R} = 161$ GeV and $m_{\tilde{e}_L} = 176$ GeV in the region 40 GeV$< M_1 < m_{\tilde{e}_R}$ for various beam polarizations [14]. We do not consider values $|M_1| > m_{\tilde{e}_R}$, where $m_{\tilde{\chi}_2^0} > m_{\tilde{\ell}_R}$, because then the two–body decay $\tilde{\chi}_2^0 \to \tilde{\ell}_R + \ell$ would be the dominant decay channel. Fig. 8b shows the analogous curves for $m_{\tilde{e}_L} = 500$ GeV. One clearly sees from the curves for left polarized electrons and/or right polarized positrons that the $\tilde{e}_L$ exchange is strongly suppressed, and one obtains higher cross sections for right polarized e^- beams.

We have also studied the M_1 dependence of the forward–backward asymmetry A_{FB} of the decay electron, eq. (23), shown in Fig. 9a and b for $m_{\tilde{e}_L} = 176$ GeV and $m_{\tilde{e}_L} = 500$ GeV. One notices a significant variation with M_1 and a strong dependence on the beam polarizations. Comparing Fig. 9a and b, one observes that in the region 40 GeV$< M_1 <$100 GeV the forward–backward asymmetries of the decay electron are different. This is due to the suppression of $\tilde{e}_L$ exchange in Fig. 9b.

Another observable which has a characteristic M_1 dependence is the polarization asymmetry defined as

$$A_{pol} = \frac{\sigma^{AB} - \sigma^{CD}}{\sigma^{AB} + \sigma^{CD}} = \frac{\sigma_e^{AB} - \sigma_e^{CD}}{\sigma_e^{AB} + \sigma_e^{CD}} \quad , \tag{27}$$

where A, C indicate two values of the polarization P_{e^-}, and B, D two values of the polarization P_{e^+}.

In Fig. 10 we show A_{pol} as a function of M_1 at $\sqrt{s} = m_{\tilde{\chi}_1^0} + m_{\tilde{\chi}_2^0} + 30$ GeV for different beam polarizations. Apart from M_1 we take the parameters and masses as in scenario A1. In the case of a small mass difference between $\tilde{e}_L$ and $\tilde{e}_R$, M_1 can be constrained by measuring A_{pol} for different beam polarizations. For larger selectron mass differences the M_1 dependence of A_{pol} is much weaker.

4 Conclusions

The objective of this paper has been twofold. Firstly, we have studied the advantage of having both the e^- and the e^+ beam polarized. If the polarizations of e^- and e^+ are varied, the cross sections depend significantly on the mixing character of the charginos and neutralinos and on the masses of $\tilde{\nu}_e$, $\tilde{e}_L$ and $\tilde{e}_R$. By an appropriate choice of polarizations one can obtain up to three times larger cross sections than in the unpolarized case. Secondly,

we have studied the forward–backward asymmetry of the decay electron in $e^+e^- \to \tilde{\chi}_1^+\tilde{\chi}_1^-$, $\tilde{\chi}_1^- \to \tilde{\chi}_1^0 e^- \bar{\nu}_e$, and in $e^+e^- \to \tilde{\chi}_1^0\tilde{\chi}_2^0$, $\tilde{\chi}_2^0 \to \tilde{\chi}_1^0 e^+e^-$ taking into account the full spin correlations between production and decay. Measuring this asymmetry for various beam polarizations gives further constraints on the masses of $\tilde{\nu}_e$, $\tilde{e}_L$ and $\tilde{e}_R$, also if direct production of these particles is kinematically not possible. It also constrains the mixing properties of the charginos and neutralinos. We have also studied the dependence on the gaugino mass parameter M_1. For a determination of M_1 the use of polarized e^+ and e^- beams would also be very useful.

Acknowledgments

We thank U. Martyn for many valuable discussions. Parts of the calculations have been performed on the QCM cluster at the University of Karlsruhe, supported by the Deutsche Forschungsgemeinschaft under contract number FOR 264/2-1. We are grateful to W. Porod and S. Hesselbach for providing the computer programs for neutralino and chargino total widths. This work was also supported by the German Federal Ministry for Research and Technology (BMBF) under contract number 05 7WZ91P (0), by the Deutsche Forschungsgemeinschaft under contract Fr 1064/4-1, and the 'Fonds zur Förderung der wissenschaftlichen Forschung' of Austria, Project No. P13139-PHY.

References

[1] A. Bartl, H. Fraas, W. Majerotto, Z.Phys. **C 30** (1986) 441; A. Bartl, H. Fraas, W. Majerotto, Nucl. Phys. **B 278** (1986) 1; A. Bartl, H. Fraas, W. Majerotto, N. Oshimo, Phys. Rev. **D 40** (1989) 1594; A. Bartl, H. Fraas, W. Majerotto, B. Mößlacher, Z.Phys. **C 55** (1992) 257; A. Bartl, W. Majerotto, B. Mößlacher, in 'e^+e^- Collisions at 500 GeV: The Physics Potential', Part B, DESY 92–123B, p. 641, ed. by P.M. Zerwas.

[2] M. Chen, C. Dionisi, M. Martinez, X. Tata, Phys.Rep. **159** (1988) 201; S. Ambrosanio et al., in *Physics at LEP2*, CERN 96-01, Vol. 1, p. 463, eds. G. Altarelli, T. Sjöstrand and F. Zwirner; E. Accomando et al., Phys. Rep. **299** (1998) 1; S. Ambrosanio, B. Mele, Phys. Rev. **D 52** (1995) 3900; S. Ambrosanio, B. Mele, Phys. Rev. **D 53** (1996) 2541.

[3] S.Y. Choi, A. Djouadi, H. Dreiner, J. Kalinowski, P. Zerwas, Eur. Phys. J. **C 7** (1999) 123; S.Y. Choi, A. Djouadi, H.S. Song, P. Zerwas,

Eur. Phys. J. **C 8** (1999) 669; V. Lafage et al., Int. J. Mod. Phys. **A14** (1999) 5075; S.Y. Choi, M. Guchait, J.Kalinowski, P.M. Zerwas, hep-ph/0001175; S.Y. Choi, A. Djouadi, M. Guchait, J. Kalinowski, H.S. Song, P.M. Zerwas, hep-ph/0002033.

[4] J.L. Kneur, G. Moultaka, Phys. Rev. **D 59** (1999) 015005.

[5] G. Moortgat–Pick, S. Hesselbach, F. Franke, H. Fraas, hep-ph/9909549, to be published in the Proceedings of 4th International Workshop on Linear Colliders (LCWS 99), Sitges, Barcelona, Spain, 28 April - 5 May 1999; S. Hesselbach, F. Franke, H. Fraas, WUE-ITP-2000-008, to be published in the Proceedings of the 2nd Joint ECFA/DESY study on Physics and Detectors for a Linear Electron-Positron Collider.

[6] S. Hesselbach, PhD Thesis, Würzburg 1999; S. Hesselbach, F. Franke, H. Fraas, hep-ph/0003272.

[7] G. Moortgat–Pick, H. Fraas, A. Bartl, W. Majerotto, Eur. Phys. J. **C 7** (1999) 113; G. Moortgat–Pick, H. Fraas, Acta Phys. Polon. **B 30** (1999) 1999.

[8] G. Moortgat–Pick, H. Fraas, Phys. Rev. **D 59** (1999) 015016.

[9] G. Moortgat–Pick, H. Fraas, A. Bartl, W. Majerotto, Eur. Phys. J. **C9** (1999) 521; Eur. Phys. J. **C9** (1999) 549 (E).

[10] G. Moortgat–Pick, PhD Thesis, Würzburg 1999, ISBN 3-8265-6981-4.

[11] H.E. Haber, G.L. Kane, Phys. Rep. **117** (1985) 75.

[12] S. Ambrosanio, G.A. Blair, P. Zerwas, ECFA-DESY LC-Workshop, 1998, http://www.desy.de/conferences/ecfa-desy-lc98.html.

[13] G. Moortgat–Pick, A. Bartl, H. Fraas, W. Majerotto, hep-ph/0004181.

[14] G. Moortgat–Pick, A. Bartl, H. Fraas, W. Majerotto, hep-ph/0002253.

[15] J. L. Feng, M. E. Peskin, H. Murayama, X. Tata, Phys. Rev. D 52 (1995) 1418.

[16] T. Tsukamoto, K. Fujii, H. Murayama, M. Yamaguchi, Y. Okada, Phys. Rev. **D 51** (1995) 3153.

[17] S.P. Martin, P. Ramond, Phys. Rev. **D 48** (1993) 5365.

[18] J.L. Feng, M.J. Strassler, Phys. Rev. **D 55** (1997) 1326.

[19] U. Martyn, G. Blair, hep-ph/9910416, to be published in the Proceedings of 4th International Workshop on Linear Colliders (LCWS 99), Sitges, Barcelona, Spain, 28 April - 5 May 1999.

	M_2	μ	$\tan\beta$	$m_{\tilde{e}_L}$	$m_{\tilde{e}_R}$	$m_{\tilde{\nu}}$	$m_{\tilde{\chi}_1^0}$	$m_{\tilde{\chi}_2^0}$	$m_{\tilde{\chi}_3^0}$	$m_{\tilde{\chi}_4^0}$	$m_{\tilde{\chi}_1^\pm}$	$m_{\tilde{\chi}_2^\pm}$
A1	152	316	3	176	132	161	71	130	320	348	128	346
A2	152	316	3	500	132	161	71	130	320	348	128	346
B	150	263	30	217	183	202	75	133	273	293	132	295

Table 1: Parameters and masses (in GeV) in scenarios A1, A2, and B.

A1	$\tilde{\chi}_1^+\tilde{\chi}_1^-(\sqrt{s}=266$ GeV)	$(-+)$	(-0)	(00)	$(--)$	$(++)$	$(+0)$	$(+-)$
	σ/fb	410	256	139	103	34	22	10
	$\tilde{\chi}_1^+\tilde{\chi}_2^-(\sqrt{s}=484$ GeV)	$(+-)$	$(+0)$	(00)	$(-+)$	(-0)	$(++)$	$(--)$
	σ/fb	6.0	3.8	2.9	2.7	1.9	1.7	1.1
	$\tilde{\chi}_2^+\tilde{\chi}_2^-$ $(\sqrt{s}=702$ GeV)	$(-+)$	(-0)	(00)	$(--)$	$(+-)$	$(+0)$	$(++)$
	σ/fb	113	72	45	30	24	19	15
B	$\tilde{\chi}_1^+\tilde{\chi}_1^-$ $(\sqrt{s}=274$ GeV)	$(-+)$	(-0)	(00)	$(--)$	$(++)$	$(+0)$	$(+-)$
	σ/fb	709	443	239	177	57	36	15
	$\tilde{\chi}_1^+\tilde{\chi}_2^-$ $(\sqrt{s}=437$ GeV)	$(+-)$	$(+0)$	(00)	$(++)$	$(-+)$	(-0)	$(--)$
	σ/fb	10.0	6.3	3.9	2.6	1.9	1.6	1.2
	$\tilde{\chi}_2^+\tilde{\chi}_2^-$ $(\sqrt{s}=600$ GeV)	$(-+)$	(-0)	(00)	$(--)$	$(+-)$	$(+0)$	$(++)$
	σ/fb	194	123	75	51	32	28	23

Table 2: Polarized cross sections $\sigma = \sigma(e^+e^- \to \tilde{\chi}_i^+\tilde{\chi}_j^-)$/fb, i, j=1, 2, at $\sqrt{s} = m_{\tilde{\chi}_i^+} + m_{\tilde{\chi}_j^-} + 10$ GeV in scenarios A1 and B, see Table 1, for unpolarized beams (00), only electron beam polarized (-0), $(+0)$ with $P_{e^-} = \pm 85\%$ and both beams polarized with $P_{e^-} = \pm 85\%$, $P_{e^+} = \pm 60\%$.

[20] S.M. Bilenky, E.C. Christova, N.P. Nedelcheva, Bulg. Jour. of Phys. **13** (1986) 283.

[21] SLAC–Report 485, submitted to *Snowmass 1996*.

[22] C. Blöchinger, H. Fraas, hep-ph/0001034.

A1	$\tilde{\chi}_1^0\tilde{\chi}_1^0(\sqrt{s}=172$ GeV)	(+−)	(+0)	(00)	(++)	(−−)	(−0)	(−+)
	σ/fb	430	269	146	108	35	23	11
	$\tilde{\chi}_1^0\tilde{\chi}_2^0(\sqrt{s}=231$ GeV)	(−+)	(−0)	(+−)	(00)	(+0)	(−−)	(++)
	σ/fb	56	36	35	30	25	17	13
	$\tilde{\chi}_1^0\tilde{\chi}_3^0$ ($\sqrt{s}=421$ GeV)	(+−)	(+0)	(00)	(++)	(−+)	(−0)	(−−)
	σ/fb	25	16	9.3	6.5	3.0	2.8	2.7
	$\tilde{\chi}_1^0\tilde{\chi}_4^0$ ($\sqrt{s}=449$ GeV)	(+−)	(+0)	(00)	(++)	(−+)	(−0)	(−−)
	σ/fb	7.9	5.0	3.2	2.1	1.7	1.4	1.0
	$\tilde{\chi}_2^0\tilde{\chi}_2^0$ ($\sqrt{s}=290$ GeV)	(−+)	(−0)	(00)	(−−)	(++)	(+0)	(+−)
	σ/fb	121	76	41	30	10	6.3	2.7
	$\tilde{\chi}_2^0\tilde{\chi}_3^0$ ($\sqrt{s}=480$ GeV)	(−+)	(−0)	(00)	(−−)	(+−)	(+0)	(++)
	σ/fb	41	26	16	11	7.2	6.1	4.9
	$\tilde{\chi}_2^0\tilde{\chi}_4^0$ ($\sqrt{s}=508$ GeV)	(−+)	(−0)	(00)	(−−)	(++)	(+0)	(+−)
	σ/fb	11	6.6	3.6	2.7	0.9	0.6	0.4
	$\tilde{\chi}_3^0\tilde{\chi}_3^0$ ($\sqrt{s}=670$ GeV)	(−+)	(+−)	(−0)	(00)	(+0)	(−−)	(++)
	σ/fb	$< 10^{-2}$ fb						
	$\tilde{\chi}_3^0\tilde{\chi}_4^0$ ($\sqrt{s}=696$ GeV)	(−+)	(+−)	(−0)	(00)	(+0)	(−−)	(++)
	σ/fb	60	41	39	34	28	18	15
	$\tilde{\chi}_4^0\tilde{\chi}_4^0$ ($\sqrt{s}=722$ GeV)	(−+)	(−0)	(00)	(−−)	(+−)	(+0)	(++)
	σ/fb	< 0.2 fb						
A2	$\tilde{\chi}_1^0\tilde{\chi}_2^0$ ($\sqrt{s}=231$ GeV)	(+−)	(+0)	(00)	(++)	(−+)	(−0)	(−−)
	σ/fb	35	22	13	9.0	4.7	4.2	3.8
B	$\tilde{\chi}_1^0\tilde{\chi}_1^0$ ($\sqrt{s}=180$ GeV)	(+−)	(+0)	(00)	(++)	(−−)	(−0)	(−+)
	σ/fb	191	119	65	48	16	10	5.7
	$\tilde{\chi}_1^0\tilde{\chi}_2^0$ ($\sqrt{s}=238$ GeV)	(−+)	(−0)	(00)	(+−)	(−−)	(+0)	(++)
	σ/fb	50	31	21	14	13	11	7
	$\tilde{\chi}_1^0\tilde{\chi}_3^0$ ($\sqrt{s}=378$ GeV)	(+−)	(+0)	(00)	(++)	(−−)	(−0)	(−+)
	σ/fb	42	26	15	11	3.9	3.4	2.9
	$\tilde{\chi}_1^0\tilde{\chi}_4^0$ ($\sqrt{s}=398$ GeV)	(+−)	(+0)	(00)	(−+)	(++)	(−0)	(−−)
	σ/fb	6.3	4.0	2.7	1.8	1.7	1.4	1.0
	$\tilde{\chi}_2^0\tilde{\chi}_2^0$ ($\sqrt{s}=296$ GeV)	(−+)	(−0)	(00)	(−−)	(++)	(+0)	(+−)
	σ/fb	59	37	20	15	4.8	3.1	1.3
	$\tilde{\chi}_2^0\tilde{\chi}_3^0$ ($\sqrt{s}=436$ GeV)	(−+)	(−0)	(00)	(−−)	(+−)	(+0)	(++)
	σ/fb	79	50	31	21	16	13	10
	$\tilde{\chi}_2^0\tilde{\chi}_4^0$ ($\sqrt{s}=456$ GeV)	(−+)	(−0)	(00)	(−−)	(++)	(+0)	(+−)
	σ/fb	11	6.9	3.7	2.7	1.0	0.6	0.3
	$\tilde{\chi}_3^0\tilde{\chi}_3^0$ ($\sqrt{s}=576$ GeV)	(−+)	(+−)	(−0)	(00)	(+0)	(−−)	(++)
	σ/fb	$< 10^{-2}$ fb						
	$\tilde{\chi}_3^0\tilde{\chi}_4^0$ ($\sqrt{s}=596$ GeV)	(−+)	(+−)	(−0)	(00)	(+0)	(−−)	(++)
	σ/fb	78	55	51	44	37	24	20
	$\tilde{\chi}_4^0\tilde{\chi}_4^0$ ($\sqrt{s}=616$ GeV)	(−+)	(−0)	(00)	(−−)	(+−)	(+0)	(++)
	σ/fb	< 0.4 fb						

Table 3: Polarized cross sections $\sigma = \sigma(e^+e^- \to \tilde{\chi}_i^0\tilde{\chi}_j^0)$/fb, i, j=1,...,4, at $\sqrt{s} = m_{\tilde{\chi}_i^0} + m_{\tilde{\chi}_j^0} + 30$ GeV in scenarios A1, A2 and B, see Table 1, for unpolarized beams (00), only electron beam polarized (−0), (+0) with $P_{e^-} = \pm 85\%$ and both beams polarized with $P_{e^-} = \pm 85\%$, $P_{e^+} = \pm 60\%$.

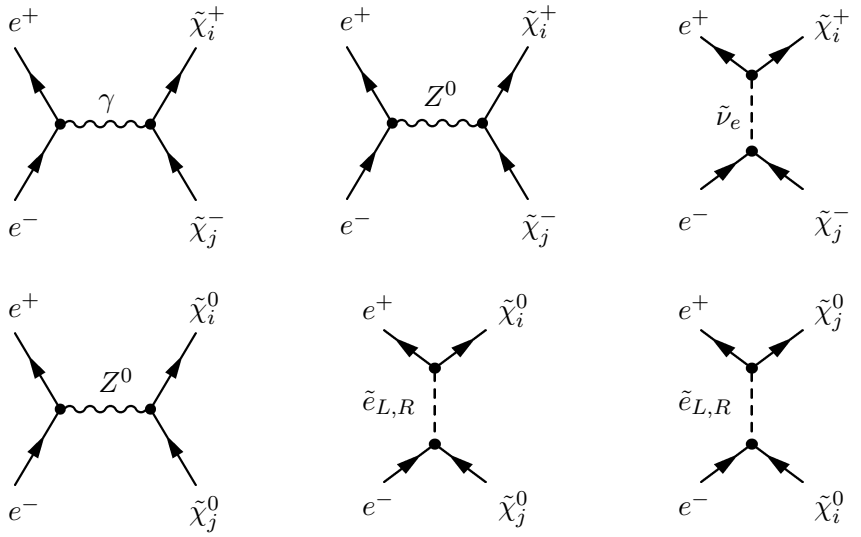

Figure 1a: Feynman diagrams for chargino production $e^+e^- \to \tilde{\chi}_i^+\tilde{\chi}_j^-$ and neutralino production $e^+e^- \to \tilde{\chi}_i^0\tilde{\chi}_j^0$.

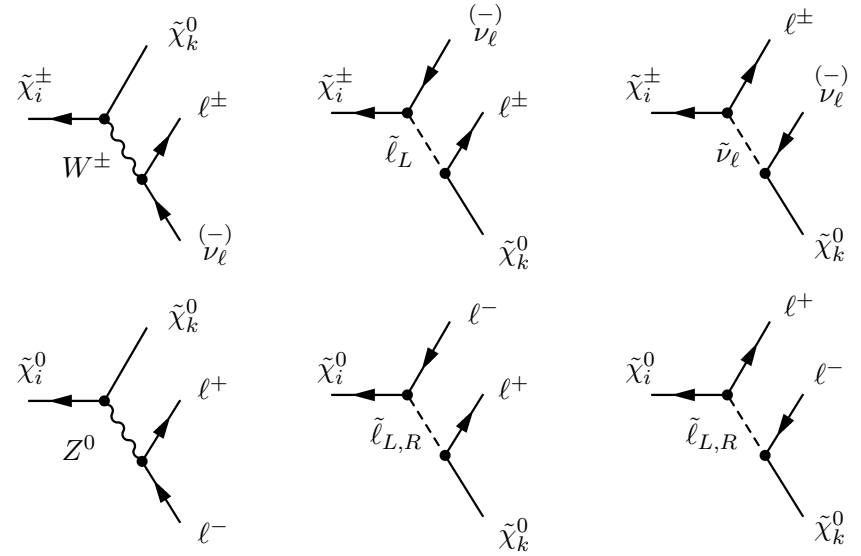

Figure 1b: Feynman diagrams for chargino decays $\tilde{\chi}_i^\pm \to \tilde{\chi}_k^0\ell^\pm \overset{(-)}{\nu}_\ell$ and neutralino decays $\tilde{\chi}_i^0 \to \tilde{\chi}_k^0\ell^+\ell^-$.

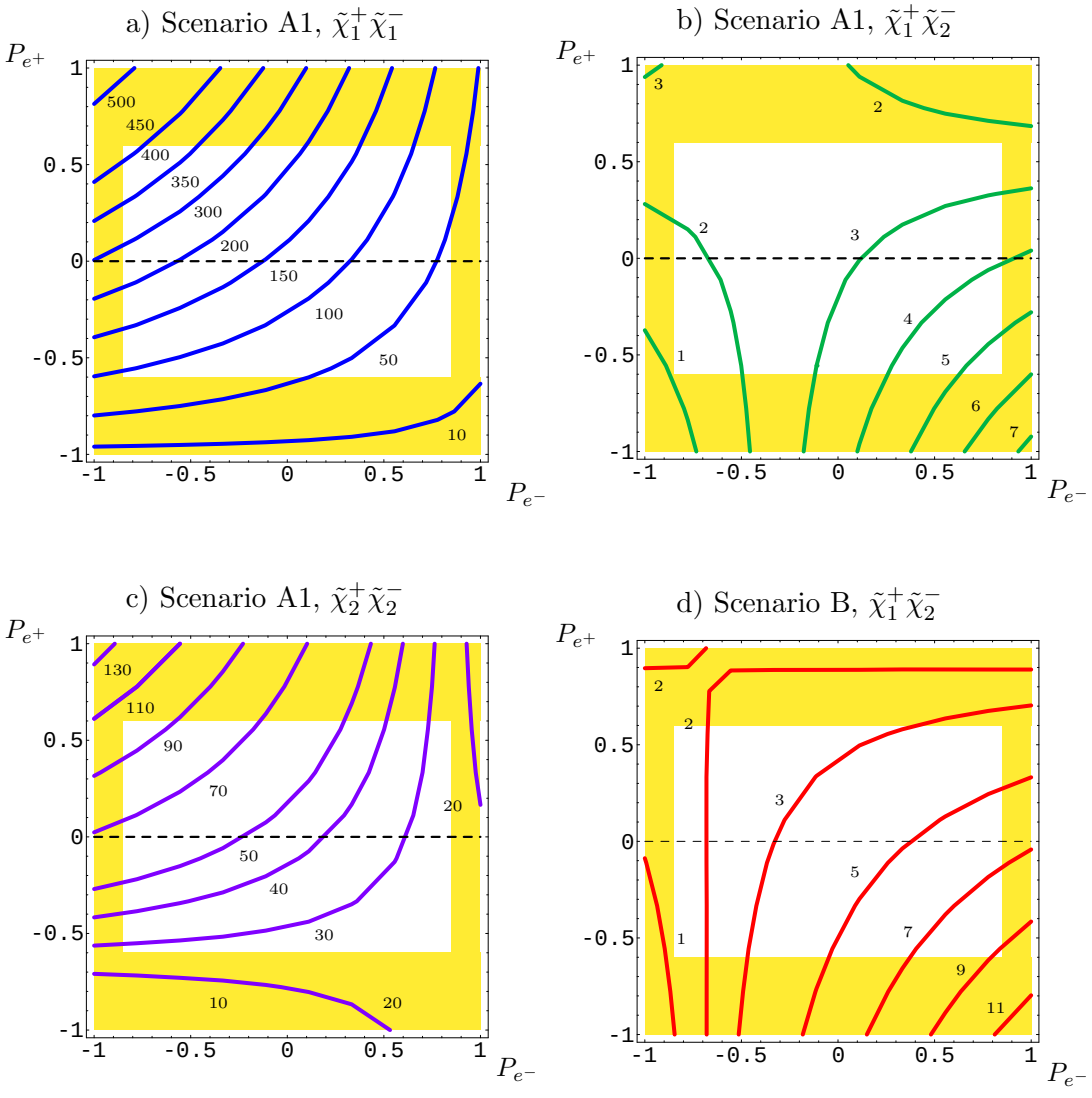

Figure 2: Contour lines of cross section $\sigma(e^+e- \to \tilde{\chi}_i^+\tilde{\chi}_j^-)$ at $\sqrt{s} = m_{\tilde{\chi}_i^+} + m_{\tilde{\chi}_j^-} + 10$ GeV. The longitudinal beam polarization for electrons (positrons) is denoted by P_{e^-} (P_{e^+}). The white region is for $|P_{e^-}| \leq 85\%$, $|P_{e^+}| \leq 60\%$ (dashed line if only the electron beam is polarized).

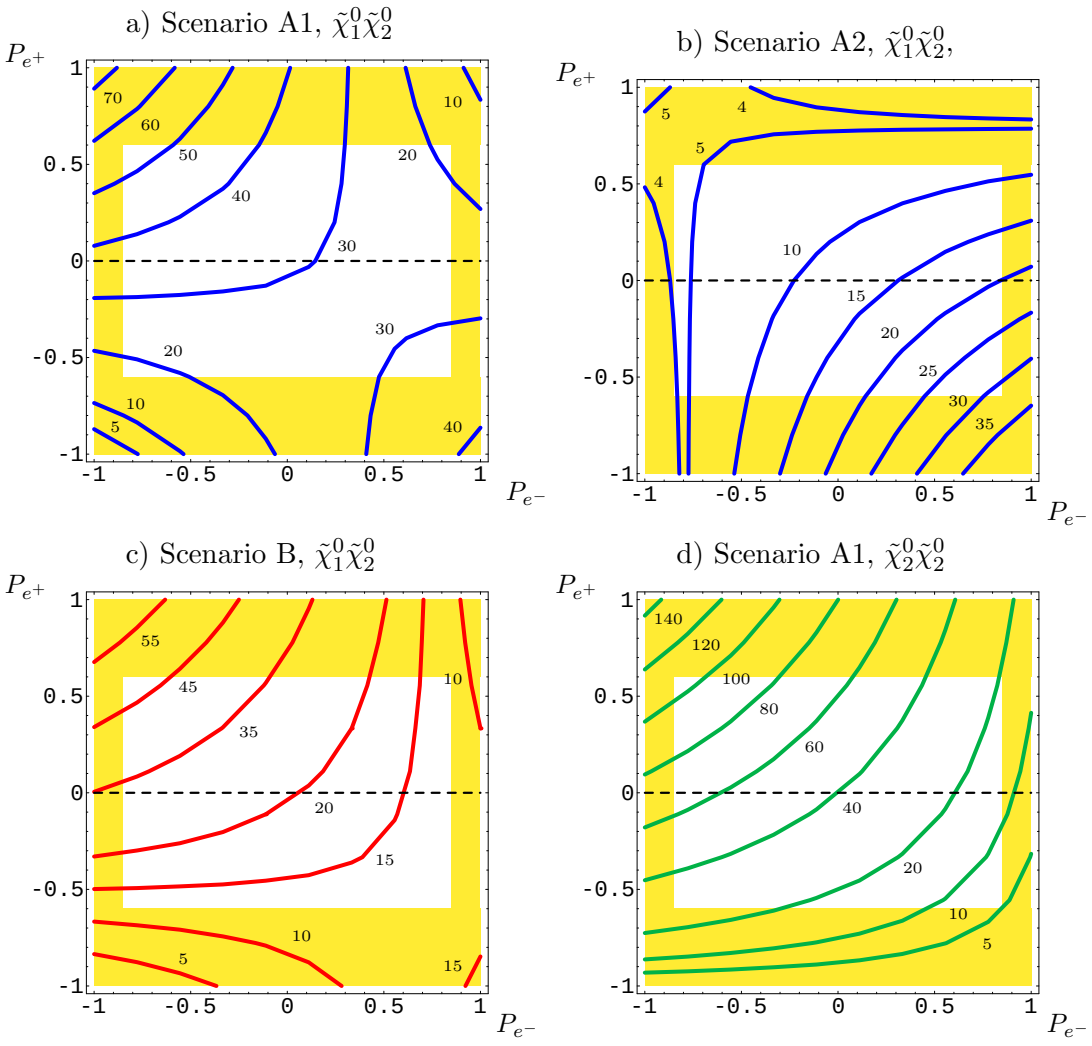

Figure 3: Contour lines of cross section $\sigma(e^+e- \to \tilde{\chi}_i^0\tilde{\chi}_j^0)$ at $\sqrt{s} = m_{\tilde{\chi}_i^0} + m_{\tilde{\chi}_j^0} + 30$ GeV in scenario A1. The longitudinal beam polarization for electrons (positrons) is denoted by P_{e^-} (P_{e^+}). The white region is for $|P_{e^-}| \leq 85\%$, $|P_{e^+}| \leq 60\%$ (dashed line if only the electron beam is polarized).

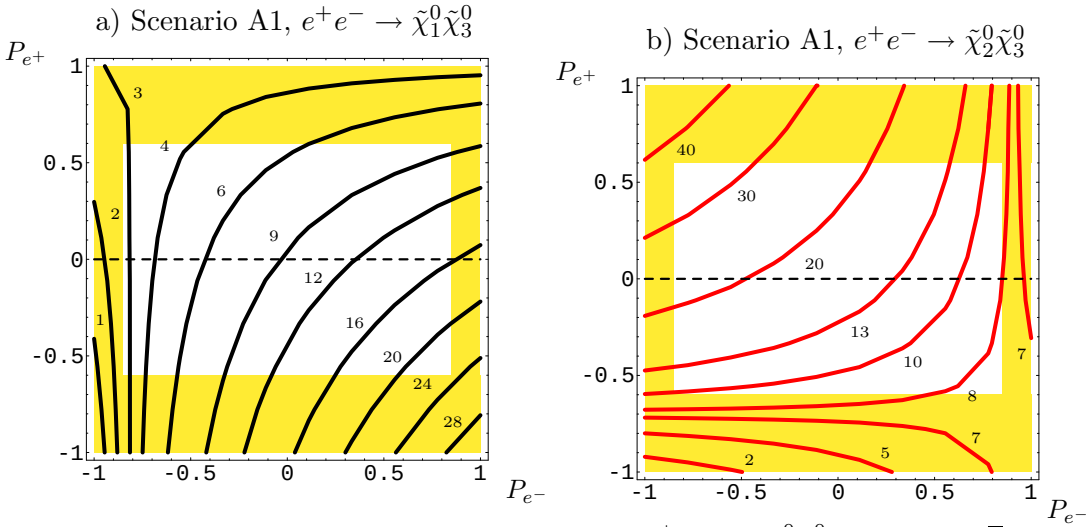

Figure 4: Contour lines of cross section $\sigma(e^+e^- \to \tilde{\chi}_i^0\tilde{\chi}_j^0)$ in fb at $\sqrt{s} = (m_{\tilde{\chi}_1^0} + m_{\tilde{\chi}_2^0}) + 30$ GeV in scenario A1. The longitudinal beam polarization for electrons (positrons) is denoted by P_{e^-} (P_{e^+}). The white region is for $|P_{e^-}| < 85\%$, $|P_{e^+}| < 60\%$ (dashed–line if only electron beam polarized).

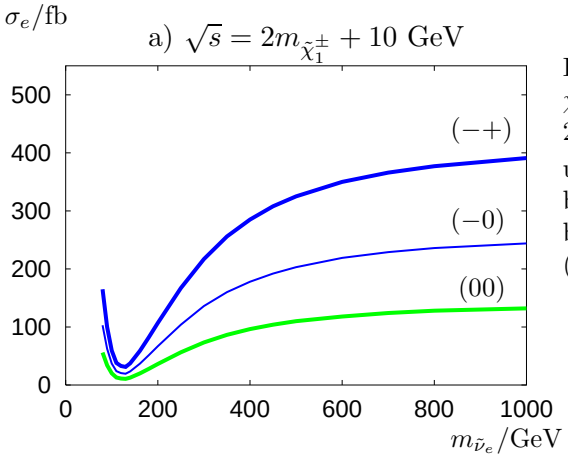

Figure 5: Cross section $\sigma_e = \sigma(e^+e^- \to \tilde{\chi}_1^+\tilde{\chi}_1^-) \times BR(\tilde{\chi}_1^- \to \tilde{\chi}_1^0 e^-\bar{\nu}_e$ in fb at $\sqrt{s} = 2m_{\tilde{\chi}_1^\pm} + 10$ GeV as function of $m_{\tilde{\nu}_e}$ for unpolarized beams (00), only the electron beam polarized $P_-^3 = -85\%$ (−0) and both beams polarized $P_-^3 = -85\%$, $P_+^3 = +60\%$ (−+). Other parameters as in scenario A1.

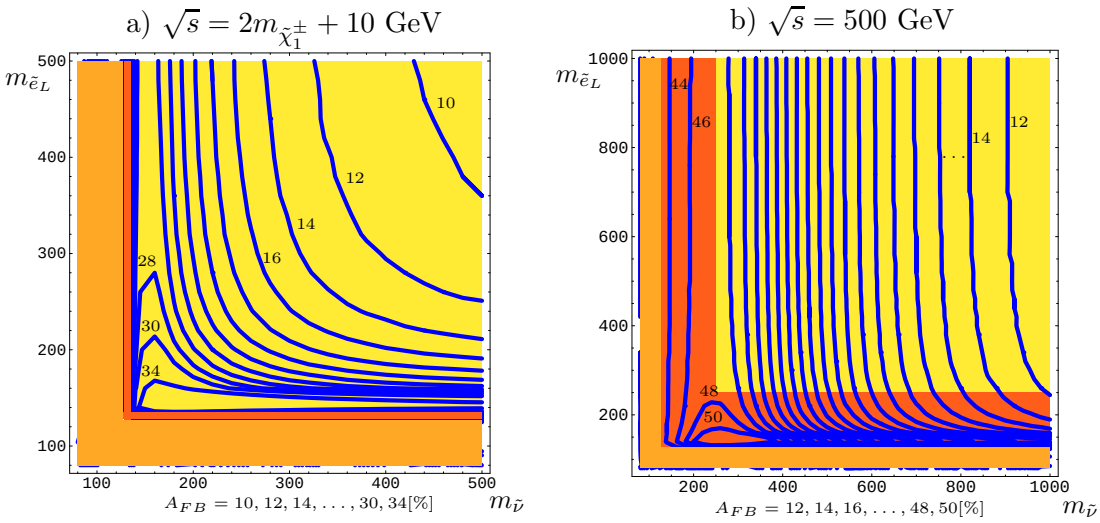

Figure 6: Contour lines of the forward–backward asymmetry of the decay electron $A_{FB}/\%$ of $e^+e^- \to \tilde{\chi}_1^+\tilde{\chi}_1^-$, $\tilde{\chi}_1^- \to \tilde{\chi}_1^0 e^- \bar{\nu}$ at a) $\sqrt{s} = 2m_{\tilde{\chi}_1^\pm} + 10$ GeV and b) $\sqrt{s} = 500$ GeV, as a function of $m_{\tilde{e}_L}$ and $m_{\tilde{\nu}}$ for $P_{e^-} = -85\%$, $P_{e^+} = +60\%$, the other parameters as in scenario A1. The light covered region is dominated by the two–body decay $\tilde{\chi}_1^- \to \tilde{e}_L\bar{\nu}_e$ or $\tilde{\chi}_1^- \to \tilde{\nu}_e e^-$. Outside the red coloured region direct production of $\tilde{e}_L$ or $\tilde{\nu}_e$ is not possible, $\sqrt{s}/2 > m_{\tilde{e}_L}, m_{\tilde{\nu}_e}$.

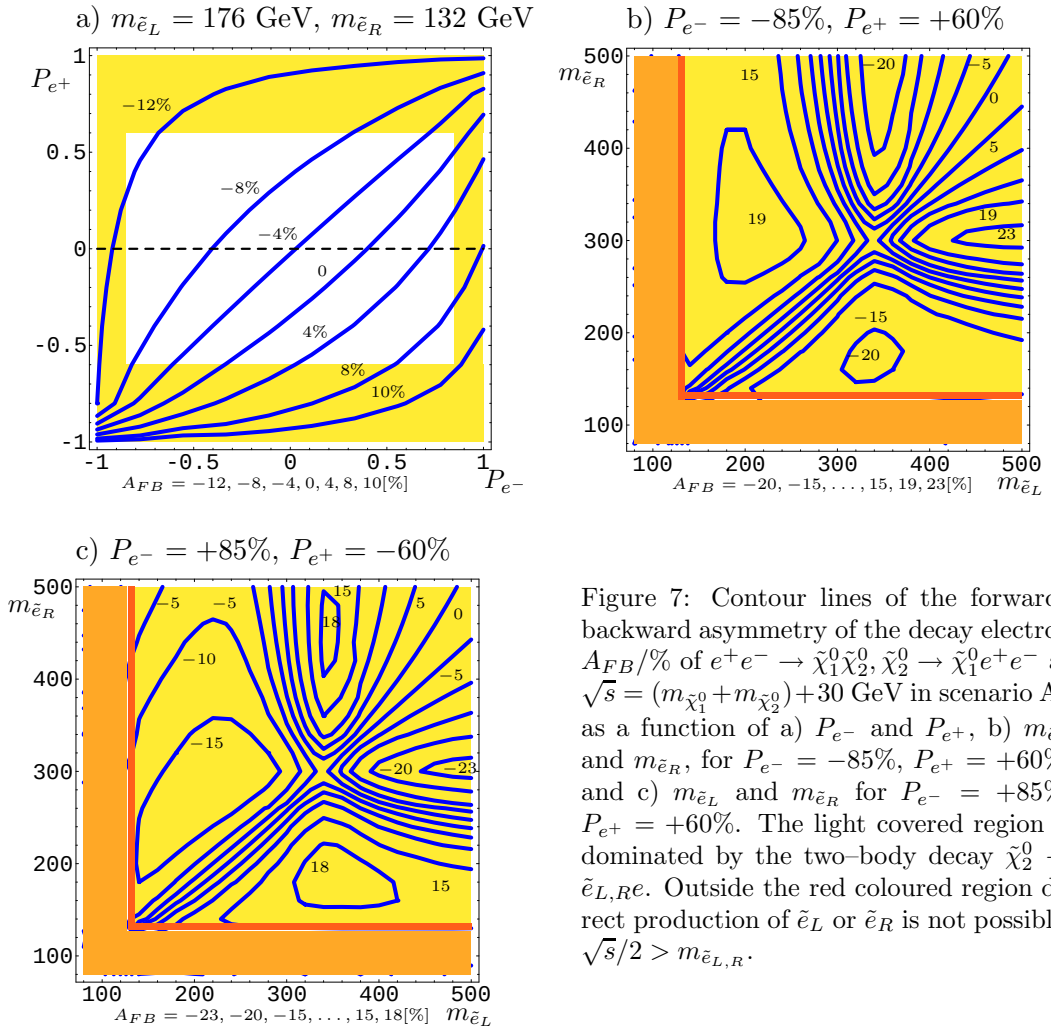

Figure 7: Contour lines of the forward–backward asymmetry of the decay electron $A_{FB}/\%$ of $e^+e^- \to \tilde{\chi}_1^0\tilde{\chi}_2^0, \tilde{\chi}_2^0 \to \tilde{\chi}_1^0 e^+e^-$ at $\sqrt{s} = (m_{\tilde{\chi}_1^0} + m_{\tilde{\chi}_2^0}) + 30$ GeV in scenario A1 as a function of a) P_{e^-} and P_{e^+}, b) $m_{\tilde{e}_L}$ and $m_{\tilde{e}_R}$, for $P_{e^-} = -85\%$, $P_{e^+} = +60\%$, and c) $m_{\tilde{e}_L}$ and $m_{\tilde{e}_R}$ for $P_{e^-} = +85\%$, $P_{e^+} = +60\%$. The light covered region is dominated by the two–body decay $\tilde{\chi}_2^0 \to \tilde{e}_{L,R} e$. Outside the red coloured region direct production of $\tilde{e}_L$ or $\tilde{e}_R$ is not possible, $\sqrt{s}/2 > m_{\tilde{e}_{L,R}}$.

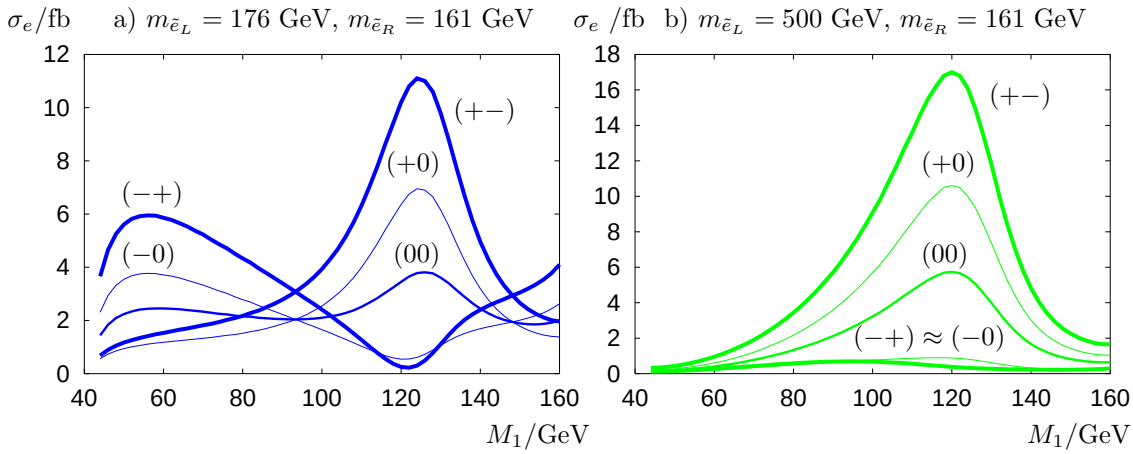

Figure 8: Cross sections σ_e at $\sqrt{s} = m_{\tilde{\chi}_1^0} + m_{\tilde{\chi}_2^0} + 30$ GeV as function of gaugino parameter M_1 for unpolarized beams (00), for only electron beam polarized (−0), (+0) with $P_{e^-} = \pm 85\%$ and for both beams polarized (−+), (+−) with $P_- = \mp 85\%$, $P_{e^+} = \pm 60\%$. The slepton masses are a) $m_{\tilde{e}_L} = 176$ GeV, $m_{\tilde{e}_R} = 161$ GeV, and b) $m_{\tilde{e}_L} = 500$ GeV, $m_{\tilde{e}_R} = 161$ GeV; the other SUSY parameters as in scenario A1.

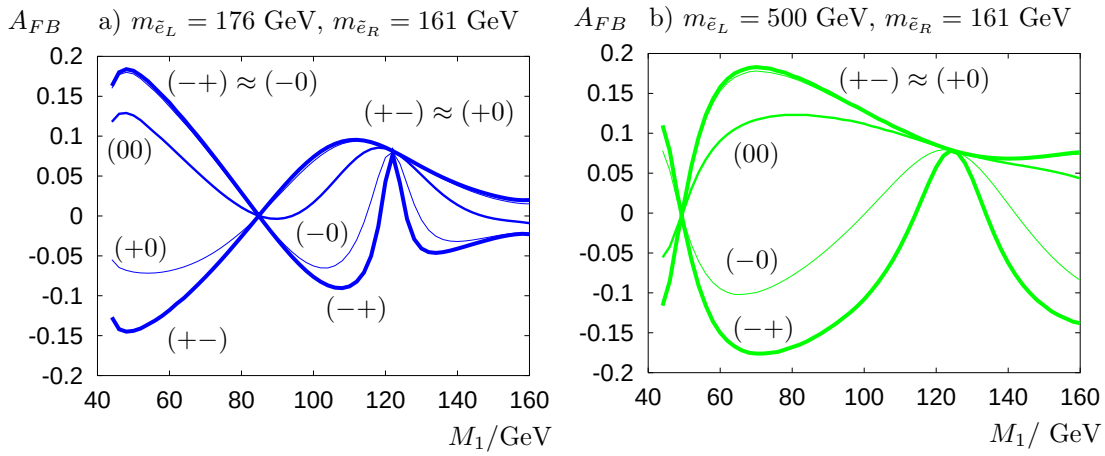

Figure 9: Forward–backward asymmetries A_{FB} of the decay electron of $e^+e^- \to \tilde{\chi}_1^0\tilde{\chi}_2^0$, $\tilde{\chi}_2^0 \to \tilde{\chi}_1^0 e^+e^-$ at $\sqrt{s} = m_{\tilde{\chi}_1^0} + m_{\tilde{\chi}_2^0} + 30$ GeV, as a function of the gaugino parameter M_1 for a) $m_{\tilde{e}_L} = 176$ GeV, $m_{\tilde{e}_R} = 161$ GeV and b) $m_{\tilde{e}_L} = 500$ GeV, $m_{\tilde{e}_R} = 161$ GeV for unpolarized beams (00), only electron beam polarized (−0), (+0) and both beams polarized (−+), (+−); the other SUSY parameters as in scenario A1.

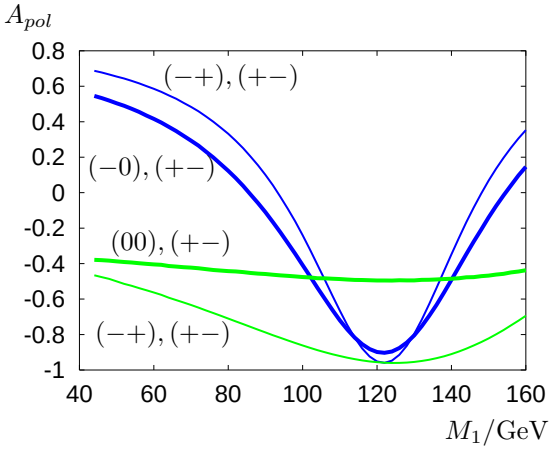

Figure 10: Polarization asymmetries A_{pol}, eq.(27), of $e^+e^- \to \tilde{\chi}^0_1\tilde{\chi}^0_2$, $\tilde{\chi}^0_2 \to \tilde{\chi}^0_1 e^+e^-$ at $\sqrt{s} = m_{\tilde{\chi}^0_1} + m_{\tilde{\chi}^0_2} + 30$ GeV as a function of the gaugino parameter M_1 for $m_{\tilde{e}_L} = 176$ GeV, $m_{\tilde{e}_R} = 161$ GeV (dark) and $m_{\tilde{e}_L} = 500$ GeV, $m_{\tilde{e}_R} = 161$ GeV (light); the other SUSY parameters as in scenario A1. $(-+)$, $(+-)$ corresponds to $A_{pol} = (\sigma_e^{-+} - \sigma_e^{+-})/(\sigma_e^{-+} + \sigma_e^{+-})$ and analogously for the other curves.